Extracting Earth's Elastic Wave Response from Noise Measurements

Roel Snieder[1] and Eric Larose[2]

[1]Center for Wave Phenomena, Colorado School of Mines, Golden, Colorado 80401; email: rsnieder@mines.edu

[2]Institut des Sciences de la Terre, CNRS and Université de Grenoble, 38041 Grenoble Cedex 9, France; email: eric.larose@ujf-grenoble.fr

Annu. Rev. Earth Planet. Sci. 2013. 41:183–206

The *Annual Review of Earth and Planetary Sciences* is online at earth.annualreviews.org

This article's doi: 10.1146/annurev-earth-050212-123936

Keywords

seismic interferometry, Green's function retrieval

Abstract

Recent research has shown that noise can be turned from a nuisance into a useful seismic source. In seismology and other fields in science and engineering, the estimation of the system response from noise measurements has proven to be a powerful technique. To convey the essence of the method, we first treat the simplest case of a homogeneous medium to show how noise measurements can be used to estimate waves that propagate between sensors. We provide an overview of physics research—dating back more than 100 years—showing that random field fluctuations contain information about the system response. This principle has found extensive use in surface-wave seismology but can also be applied to the estimation of body waves. Because noise provides continuous illumination of the subsurface, the extracted response is ideally suited for time-lapse monitoring. We present examples of time-lapse monitoring as applied to the softening of soil after the 2011 Tohoku-oki earthquake, the detection of a precursor to a landslide, and temporal changes in the lunar soil.

1. INTRODUCTION

The retrieval of the seismological response of a system, such as Earth, from recorded noise is a field that has experienced explosive growth over the past decade. Traditionally, seismologists use point sources, such as earthquakes or controlled sources, to probe Earth's interior. The response to such sources that are localized in space and are temporally impulsive is termed the impulse response, or Green's function. We show in this review how the impulse response can be inferred from noise measurements. The ability to use ambient noise as a seismic source has changed many aspects of seismology. At the annual meeting of the American Geophysical Union, one can now hear seismologists make statements such as "we carefully removed data that are contaminated by earthquakes." This is a sure sign that something new has happened in seismology.

The technique of extracting the impulse response from noise measurements is known by different names that include Green's function extraction, Green's function retrieval, and seismic interferometry (all terms are used in this review). This field has been the topic of review articles (Curtis et al. 2006, Larose et al. 2006a, Galetti & Curtis 2012), tutorials (Wapenaar et al. 2010a,b), special issues of journals (Song 2010, Campillo et al. 2011), a collection of reprints (Wapenaar et al. 2008a), and a textbook (Schuster 2009). In this review, we restrict ourselves to solid Earth seismology, but important contributions to Green's function extraction have been made in a variety of other fields that include helioseismology (Duvall et al. 1993, Rickett & Claerbout 2000), ultrasound (Weaver & Lobkis 2001, 2003a,b; Malcolm et al. 2004; Larose et al. 2006b; van Wijk 2006), infrasound (Haney 2009), ocean acoustics (Roux et al. 2004, 2011; Sabra et al. 2005c), engineering (Sabra et al. 2008, Duroux et al. 2010), structural engineering (Snieder & Şafak 2006, Snieder et al. 2006a, Kohler et al. 2007, Prieto et al. 2010), and medical diagnostics (Sabra et al. 2007, Gallot et al. 2011).

This overview contains the following elements. In Section 2, we show the essence of Green's function extraction for the simplest example of acoustic waves in a homogeneous medium. The principle of extracting the system response from noise goes back more than a century, and we present an overview of the developments in physics in Section 3. Section 4 features a historical overview of developments in seismology. Retrieving body waves has proven to be much more difficult than extracting surface waves, and we discuss this discrepancy in Section 5. A particularly promising application of Green's function retrieval is monitoring because one can get the Earth response on a quasi-continuous basis (see Section 6), and we show examples of time-lapse monitoring as applied to the softening of the soil by an earthquake, the detection of a precursor to a landslide, and temporal changes in the lunar response.

2. SIMPLEST CASE: WAVE PROPAGATION IN A HOMOGENEOUS MEDIUM

We first explain the principle of the extraction of the wave response from noise for the simplest case of a homogenous medium in one, two, or three dimensions (**Figure 1**). In all cases we consider receivers A and B that are separated over a distance R and carry out the analysis in the frequency domain where the wave number at angular frequency ω is denoted by k.

We focus first on one dimension, as shown in **Figure 1*a***. The receiver B is at $x = 0$, and receiver A is at $x = R$. Random waves with spectrum $S_{\rm L}$ are incident from the left, and waves with spectrum $S_{\rm R}$ are incident from the right. The total wave field is given by $u(x) = S_{\rm L}e^{ikx} + S_{\rm R}e^{-ikx}$. The waves recorded at the two receivers are thus given by

$$u_A = S_{\rm L}e^{ikR} + S_{\rm R}e^{-ikR}, \quad u_B = S_{\rm L} + S_{\rm R}. \tag{1}$$

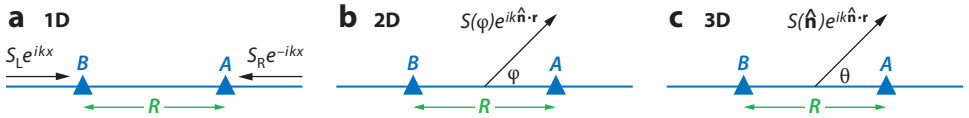

Figure 1

Two receivers A and B separated over a distance R in (*a*) one dimension, (*b*) two dimensions, and (*c*) three dimensions.

Correlation of these signals corresponds in the frequency domain to the product $u_A u_B^*$, where the asterisk denotes complex conjugation (see equation 15.52 of Snieder 2004a). The spectra of the incident waves are random variables, and we denote the expectation value by angled brackets $\langle \cdots \rangle$. When the noise incident from the left is uncorrelated with the noise incident from the right, and has the same power spectrum, then

$$\langle |S_L|^2 \rangle = \langle |S_R|^2 \rangle = \langle |S|^2 \rangle \quad \text{and} \quad \langle S_L S_R^* \rangle = \langle S_L^* S_R \rangle = 0. \tag{2}$$

Under these assumptions, the expectation value $\langle u_A u_B^* \rangle$ of the cross correlation recorded at the two stations reduces to

$$\langle u_A u_B^* \rangle = \langle |S|^2 \rangle (e^{ikR} + e^{-ikR}). \tag{3}$$

The Green's function of a one-dimensional (1D) homogenous medium is given by $G_{1D}(R, \omega) = (-i/2k) \exp(ikR)$ (Snieder 2004a). Using this in Equation (3) gives

$$\langle u_A u_B^* \rangle = 2ik \langle |S|^2 \rangle [G_{1D}(R, \omega) - G_{1D}^*(R, \omega)]. \tag{4}$$

This means that if one knows the power spectrum of the noise, one can obtain the difference $G - G^*$ of the Green's function and its complex conjugate by the cross correlation of field fluctuations. The amplitude spectrum of the noise needs to be known, but its phase spectrum does not. The difference $G(R, \omega) - G^*(R, \omega)$ corresponds in the time domain to $G(R, t) - G(R, -t)$. The Green's function is causal; hence $G(R, t)$ is nonzero only for positive time $t > 0$, and $G(R, -t)$ is only nonzero for $t < 0$. By parsing these two solutions, one can retrieve the full Green's function.

We next consider the case of a homogeneous medium in two dimensions (**Figure 1*b***). The receivers are at locations $\mathbf{r}_B = (0, 0)$ and $\mathbf{r}_A = (R, 0)$, respectively. A superposition of plane waves $e^{ik\hat{\mathbf{n}}\cdot\mathbf{r}}$ with random spectrum $S(\varphi)$ propagating in the direction $\hat{\mathbf{n}} = (\cos\varphi, \sin\varphi)$ strikes the two receivers. The total wave field recorded at the receivers is given by

$$u_A = \int_0^{2\pi} S(\varphi) e^{ikR\cos\varphi} d\varphi, \quad u_B = \int_0^{2\pi} S(\varphi') d\varphi'. \tag{5}$$

When the plane waves coming in from different directions are uncorrelated and each has a power spectrum independent of the angle of incidence, $\langle S(\varphi) S^*(\varphi') \rangle = |S|^2 \delta(\varphi - \varphi')$, and the average cross correlation is given by

$$\langle u_A u_B^* \rangle = |S|^2 \varphi \int_0^{2\pi} e^{ikR\cos\varphi} d\varphi. \tag{6}$$

We show in Appendix A that this integral is equal to

$$\langle u_A u_B^* \rangle = 4i\pi |S|^2 [G_{2D}(R, \omega) - G_{2D}^*(R, \omega)], \tag{7}$$

where $G_{2D}(R, \omega)$ is the Green's function in a homogeneous 2D medium. This expression has the same form as Equation (3) for one dimension. A time-domain version of this derivation has been given by Roux et al. (2005b). For completeness, we show in Appendix A that for a homogeneous

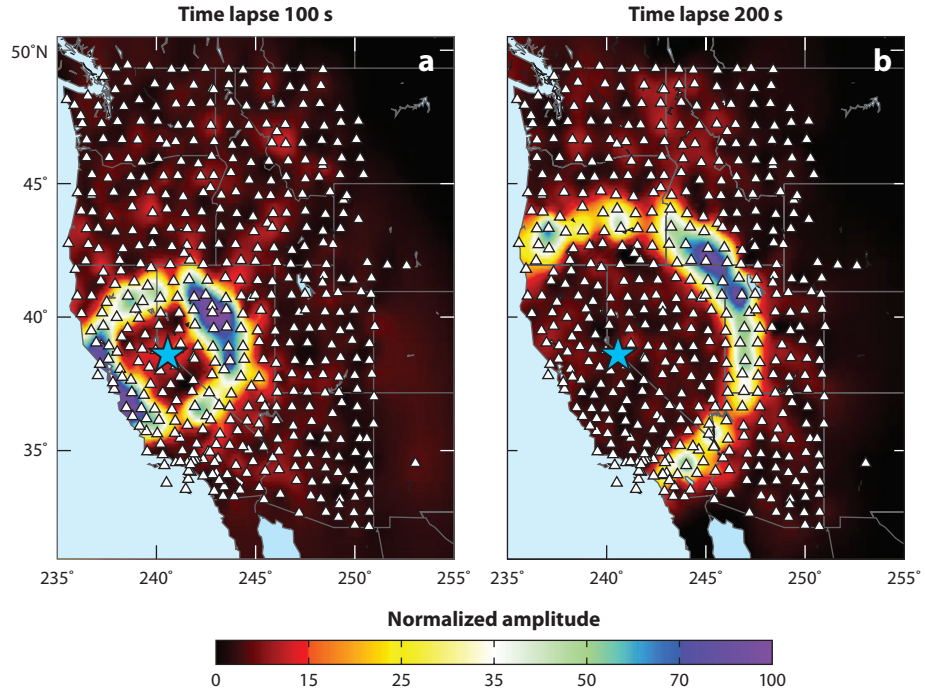

Figure 2

Noise recorded at a master station (*light blue star*) is cross-correlated with noise measured at all other USArray stations (*small white triangles*) for a lapse time of (*a*) 100 s and (*b*) 200 s. This results in surface waves that emanate from the master station. Adapted from Lin et al. (2009).

medium in three dimensions, the equation

$$\langle u_A u_B^* \rangle = 8i\pi |S|^2 [G_{3D}(R, \omega) - G_{3D}^*(R, \omega)] \quad (8)$$

holds true, with $G_{3D}(R, \omega) = -\exp(ikR)/(4\pi R)$.

We first illustrate with a data example that the Green's function in 2D indeed follows from cross correlation of recorded noise. **Figure 2** shows the cross correlation of noise recorded at USArray stations for two different lag times. The noise at a master station is cross-correlated with noise recorded at all other stations after the result is interpolated on a regular grid. The noise that was used is excited by waves in the ocean (Webb 1998); this noise is most pronounced for periods between 5 and 10 s. The spherical wavefront that emanates from the master station propagates with the velocity of the fundamental-mode Rayleigh wave. The master station acts as if a source is present. Because there is no physical source at the master station, this station acts as a virtual source (Bakulin & Calvert 2006).

There is no magic in Green's function extraction from noise in the sense that one can use data processing of recorded noise to retrieve a wave that propagates between receivers only if there is a physical wave that propagates between receivers. An ideal point source would give a spherical wavefront with constant amplitude [see Equation (7)], but the wavefronts in **Figure 2** show variations in amplitude. These variations are due to variations in the strength of the incoming oceanic noise as a function of azimuth. Studies using arrays have shown that oceanic noise is generated mostly by storms in the oceans (Schulte-Pelkum et al. 2004, Gerstoft et al. 2006, Stehly et al. 2006). Because of the localized nature of storms, the oceanic noise is, in practice, not isotropic.

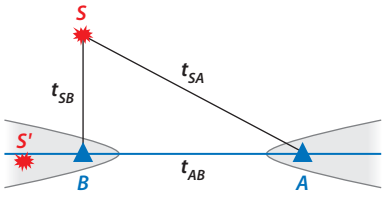

Figure 3

The stations A and B in two dimensions and the stationary phase regions for sources (*shaded gray areas*).

Fortunately, the fact that the noise is not isotropic is not necessarily a problem. We illustrate this with **Figure 3**. Consider first the noise source S. The travel time of a wave propagating between the receivers is denoted by t_{AB}, whereas the travel times of waves from source S to receivers A and B are denoted by t_{SA} and t_{SB}, respectively. Cross correlation corresponds to taking the time difference of the signals that are analyzed; hence the noise generated by source S gives, after cross correlation, a wave arriving at time $t_{SA} - t_{SB}$. In general, $t_{SA} - t_{SB} \neq t_{AB}$, so the contribution of source S does not correspond to a wave propagating between the receivers. As a consequence, the contribution of source S should vanish upon integration over all sources. So how is a wave arriving at time t_{AB} generated? Consider the noise source S' on the left. This source launches a wave that first propagates to receiver B and then continues to receiver A. The cross correlation of this wave recorded at the two receivers gives a wave arriving at the correct time: $t_{AB} = t_{S'A} - t_{S'B}$. There is a mathematical reason why, in the end, the noise source S' gives the correct contribution to the retrieval, whereas the noise source S does not contribute. Consider first source S'. When we change the location of this source a little bit, the travel time difference of the waves traveling to both receivers does not change. This means that source S' is at a stationary phase position. In contrast, when the location of S is moved, the travel time difference $t_{SA} - t_{SB}$ varies to first order in the location of the source position. The source S thus is not at a stationary phase position. When oscillatory functions are integrated, the dominant contribution comes from stationary phase positions (Bleistein & Handelsman 1975, Bleistein 1984, Snieder 2004a). This means that upon integration over all sources, the dominant contribution comes from the coherency zone (Larose 2006) or the end-fire lobes (Roux et al. 2004) (see **Figure 3**). Sources in this zone launch waves in the right direction to propagate between the receivers and lead to the extraction of G_{AB} (Snieder 2004b). For inhomogeneous media, using the equations of kinematic and dynamic ray tracing, it has been shown that the sources that lie in stationary phase regions dominate in the extraction of the Green's function (Snieder et al. 2006b). In general, the stationary phase regions launch waves along the same rays that propagate to the two receivers (see appendix A of Wapenaar et al. 2010a). For each reflected wave, a stationary phase region gives the dominant contribution to the extraction of the reflected wave by cross correlation (Snieder et al. 2006b).

3. THE BROADER PICTURE: HISTORY OF THE FLUCTUATION RESPONSE THEOREM

The principle of extracting the response of a system from noise dates back more than a century to the seminal paper of Einstein (1906) on Brownian motion. Consider first **Figure 4*a***, which shows a heavy particle, such as a smoke particle, that is suspended in air. The particle is bombarded by air molecules, and as a result, the smoke particle moves in a random way. Its motion is described by a diffusion constant D that characterizes the Brownian motion. The motion of the particle depends, of course, on the kinetic energy of the air molecules, and the diffusion constant is proportional to

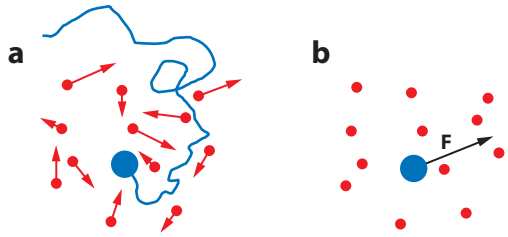

Figure 4

(*a*) When gas molecules (*red dots*) bombard a heavy smoke particle (*blue circle*), the particle executes a Brownian motion characterized by a diffusion constant D. (*b*) When the same smoke particle is kicked by a force **F**, it slows down because of the viscosity γ of the air.

the thermal energy $k_B T$ of the air, where k_B is Boltzmann's constant. **Figure 4*b*** shows the same smoke particle suspended in air, but now the particle is kicked by a force **F**. As a result, the particle moves but is slowed down by the viscosity γ of the air. Einstein (1906) established the relation between the diffusion constant D and the viscosity γ. The diffusion constant characterizes the response of the smoke particle to a random forcing, whereas the viscosity characterizes the response of the particle to an external force. Implicitly, the viscosity determines the Green's function of the motion of the smoke particle; hence the work of Einstein established the connection between the response of a system to a random excitation and its Green's function.

Johnson (1928) carried out measurements of the voltage fluctuations of resistors and found that the voltage fluctuations of a resistor satisfy

$$\langle V^2/R \rangle \sim k_B T\,, \tag{9}$$

where V denotes voltage; R, electrical resistance; k_B, Boltzmann's constant; and T, absolute temperature. Nyquist (1928) explained this proportionality from the principle of thermal equilibrium. Thermal fluctuations cause voltage fluctuations that result in a current $I = V/R$. The associated power dissipation in the resistor is given by $P = VI = V^2/R$. Equation (9) thus captures the balance between the power dissipated in the resistor and the thermal energy. In statistical mechanics, the thermal energy is what leads to field fluctuations. After World War II, general proofs showed that the response of a quantum mechanical system to an impulsive excitation—the Green's function—is proportional to the cross correlation of field fluctuations caused by thermal noise (Callen & Welton 1951, Greene & Callen 1951). This principle was later formalized by Kubo (1966) as the fluctuation dissipation theorem. Tatarskii (1987) recognized that the distinction between a system and its noise is artificial and considered the fluctuation dissipation theorem by dividing the whole physical system into the system of interest (e.g., the smoke particle) and the rest of the world. Rytov et al. (1989) give a comprehensive treatment of fluctuations of electromagnetic fields and their relation to the electromagnetic response of a system.

There exists a general connection between the fluctuations in a system in thermal equilibrium and that system's response (Le Bellac et al. 2004). Suppose one has a thermodynamic system characterized with variables A_i, which are associated with conjugate variables λ_i that act as control parameters. As shown in Appendix B, the expectation values of A_i satisfy

$$\frac{\partial \langle A_i \rangle}{\partial \lambda_j} = \langle (A_i - \langle A_i \rangle)(A_j - \langle A_j \rangle) \rangle. \tag{10}$$

The left-hand side of Equation (10) gives the change in the expectation value $\langle A_i \rangle$ as the control parameter λ_j is varied. This derivative denotes the response of the system to a perturbation. The right-hand side gives the covariance of the variables A_i and A_j. This quantity characterizes the

fluctuations of the system. Equation (10) thus relates the response of the system to the fluctuations of the system; for this reason, the expression is the mathematical formulation of the fluctuation response theorem (Le Bellac et al. 2004). The retrieval of the system response thus follows from general thermodynamic principles. The value of the thermal excitation is, however, tiny compared with the energy of macroscopic motion in Earth. At a temperature of 300 K, the thermal energy is $k_B T = 4 \times 10^{-21}$ J, which is, for example, negligible compared with the energy of dropping a 1-g weight from a 1-m height ($mgh = 10^{-2}$ J). This implies that one needs macroscopic, nonthermal sources to explain the retrieval of the Earth response from recorded noise.

The retrieval of the Green's function of a general system from cross correlation of field fluctuations has been shown using derivations that do not rely on thermodynamic arguments (Wapenaar et al. 2006, Snieder et al. 2007, Gouédard et al. 2008, Weaver 2008). Green's function extraction from field fluctuations can be applied to diffusion problems (Snieder 2006), and the principle holds even for potential field problems (Slob et al. 2010, Snieder et al. 2010). In the latter application, the Green's function is static but can still be retrieved from the correlation of field fluctuations caused by time-dependent sources. For electric problems, theory requires that such sources are electric dipoles. This requirement is fortunate because fluctuations in a system do not create charges (monopoles); rather, a charge separation creates an electric dipole. Random electric bursts have been observed to be caused by fluid flow through rock samples (Haas & Revil 2009).

4. HISTORY IN SEISMOLOGY

Many of the discoveries in seismology were made by Keiiti Aki and Jon Claerbout, who were often several decades ahead of their time. Aki (1957) proposed to use ambient noise to extract surface waves propagating in the near surface. Instead of using cross correlation, he used the cross coherence of signals u_A and u_B that is defined as

$$H_{AB}(\omega) = \left\langle \frac{u_A(\omega) u_B^*(\omega)}{|u_A(\omega)||u_B(\omega)|} \right\rangle. \tag{11}$$

Because Aki employed normalization with the amplitude spectrum, this measure corrects for fluctuations in amplitude. When waves are incident with equal power from all directions, the cross coherence gives the surface wave's Green's function. This equation follows the same steps as those taken in the derivation of Equation (7).

Claerbout (1968) studied the relation between the reflection response and transmission response of a 1D layered acoustic medium. The transmission coefficient of a wave propagating vertically upward through such a stack of layers is denoted by T, and the reflection coefficient of a wave that propagates downward is denoted by R (see **Figure 5**). Claerbout (1968) showed that

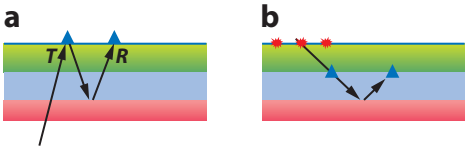

Figure 5

(*a*) Definition of the transmission coefficient T and reflection coefficient R. The reflection coefficient accounts for the total reflection response of the stack of layers. (*b*) Extracting the body waves that propagate between buried receivers (*blue triangles*) that are excited by sources at the surface.

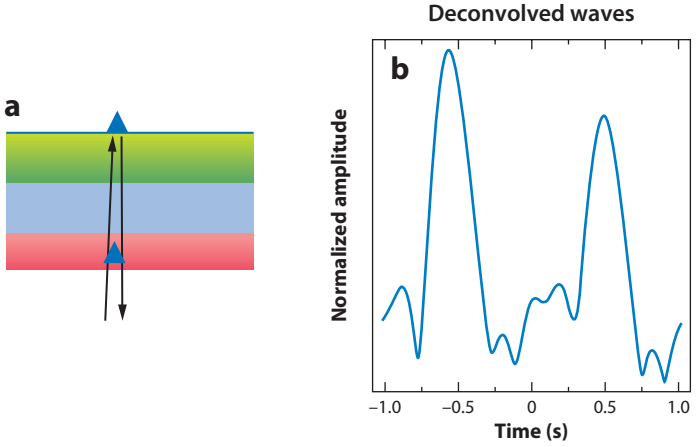

Figure 6

(*a*) Geometry of waves propagating up and down a borehole. (*b*) Deconvolution of waves recorded in the borehole with those recorded at the surface for an earthquake in the Rhine Graben recorded at a distance of 43 km (Trampert et al. 1993).

these coefficients are, in the frequency domain, related by

$$1 + R(\omega) + R^*(\omega) = T(\omega)T^*(\omega). \tag{12}$$

This equation is exact and contains all internal multiples in the stack of layers. Consider waves with complex spectrum $S(\omega)$ that are incident on the stack of layers from below. The transmitted wave recorded at the surface is then given by $u(\omega) = T(\omega)S(\omega)$. Inserting this in Equation (12) gives

$$1 + R(\omega) + R^*(\omega) = \frac{1}{|S(\omega)|^2}\langle u(\omega)u^*(\omega)\rangle. \tag{13}$$

This expression relates the reflected waves to the average cross correlation of transmitted waves. The power spectrum of the incident waves needs to be known, but the phase spectrum does not. This was the earliest example of retrieving the reflection response from the cross correlation of waves with an unknown phase spectrum. Scherbaum (1987) extended the analysis of Claerbout (1968) to SH waves with nonzero angles of incidence.

Trampert et al. (1993) deconvolved earthquake recordings taken in a borehole with measurements at the surface. Instead of using cross correlation or cross coherence, they used the following measure:

$$D_{AB}(\omega) = \left\langle \frac{u_A(\omega)}{u_B(\omega)} \right\rangle. \tag{14}$$

They showed that this equation gives the wave that travels from the borehole sensor to the surface sensor, along with the wave reflected by the free surface that propagates from the surface to the borehole sensor (**Figure 6*a***). They applied this measure to the ground motion due to an earthquake in the Rhine Graben, and the resulting deconvolved waveforms are shown in **Figure 6*b***. The wave associated with the negative times is the wave that propagates from the borehole sensor to the surface sensor, and the wave associated with the positive times is the reflected wave that propagates downward to the borehole sensor. The travel times are identical, as they should be, but the amplitudes are different. This difference is due to attenuation losses, and the amplitude ratio of these waves can be used to estimate the quality factor Q. Because the two waves are recorded at the same seismometer, this estimation is not contaminated by uncertainties in instrument calibration

or instrument coupling. This technique was later applied to measurements taken with arrays in boreholes (Mehta et al. 2007b,c) and to the vibrations of buildings (Snieder & Şafak 2006, Snieder et al. 2006a, Kohler et al. 2007, Prieto et al. 2010).

The work of Lobkis & Weaver (2001) gave the field of estimating the system response from noise measurements much visibility in seismology. They provided a beautiful derivation showing that cross correlation of recorded noise leads to the Green's function. Their derivation was based on normal-mode theory, a language that is natural for seismologists. Lobkis & Weaver (2001) also presented ultrasound measurements taken on an irregularly shaped aluminum block that beautifully confirmed their theory. In subsequent papers, they showed additional laboratory measurements that confirmed the ability to extract the Green's function from field fluctuations (Weaver & Lobkis 2001, 2003a,b). They also extended their earlier derivation based on normal modes of closed systems to open systems, in which uncorrelated noise is incident from all directions (Weaver & Lobkis 2005).

Campillo & Paul (2003) applied the concept of Green's function retrieval to coda waves of earthquakes at the western margin in Central America, recorded at stations in Mexico. They showed that by this procedure, one can extract the surface waves that propagated between the two stations. They showed experimentally that they could retrieve all components of the Green's tensor for surface waves by cross-correlating the coda waves recorded at different components at the two stations; this was later explained theoretically (Snieder 2004b).

Several subsequent studies confirmed that the fundamental-mode surface waves could be extracted successfully (Shapiro & Campillo 2004, Paul et al. 2005, Sabra et al. 2005a). The surface-wave noise appeared to be strongest for periods between 5 and 10 s, which is the frequency band of microseismic noise generated in the oceans (Webb 1998). In addition, it was shown that surface waves could be extracted for periods as large as several tens of seconds (Shapiro & Campillo 2004) and that surface waves for the Earth's hum could even be extracted for a period of approximately 200 s (Nishida et al. 2009). One of the spectacular successes of seismic interferometry was that the surface waves could be extracted so robustly. With the advent of dense arrays, such as the USArray, seismic interferometry could be used to extract the surface waves that propagate between each pair of sensors. It was applied first to stations in Southern California (Sabra et al. 2005b, Shapiro et al. 2005) and provided unprecedented illumination for surface-wave tomography. Surface waves at periods of microseismic noise (5–10 s) sample the upper 30 km; hence these noise studies revolutionized tomography of Earth's crust as evidenced by an explosive growth in the number of crustal studies based on surface waves extracted from noise (e.g., Yao et al. 2006, Lin et al. 2008, Yang & Ritzwoller 2008, Ekström et al. 2009, Li et al. 2009, Moschetti et al. 2010). A comprehensive overview of this field is given by Ritzwoller et al. (2011). Surface waves extracted from noise have also been used at lower frequencies to determine global Earth structure (Nishida et al. 2009) and at higher frequencies to image the shear-wave velocity in the near surface (Halliday et al. 2008, Bussat & Kugler 2011, de Ridder & Dellinger 2011). The dominance of surface waves in the response estimated from noise cross correlations has been used to suppress surface waves in exploration seismology (Halliday et al. 2007, Xue et al. 2009).

Recent studies have used cross coherence, as originally proposed by Aki (1957), to estimate attenuation (Prieto et al. 2009, Lawrence & Prieto 2011). For nonattenuating media, it suffices to have noise sources on a closed surface surrounding the receivers, but for attenuating media, noise must be present throughout the medium with a strength proportional to the local attenuation (Roux et al. 2005b, Snieder 2007). Tsai (2011) gives a detailed overview of the sources used for Green's function extraction in the presence or absence of attenuation.

Earthquake signals are usually much stronger than recorded noise, which is why earthquakes used to be the seismic source employed to probe deep Earth structure. Suppressing the large

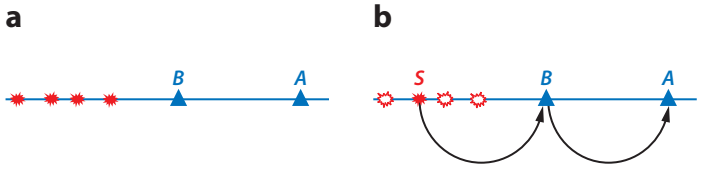

Figure 7

(*a*) For surface waves, noise sources (*solid red stars*) can be located anywhere on the receiver line. (*b*) For body waves, only the source *S* (*solid red star*), and not the other noise sources (*hollow red stars*), gives the body wave that propagates between the receivers.

contributions of earthquake signals to the cross correlation is important because these signals violate the requirement that noise sources are distributed around the receivers. An effective way of suppressing such large amplitude signals is one-bit filtering (Larose et al. 2004), whereby the signal is replaced with +1 if the amplitude is positive and with −1 if the amplitude is negative. Perhaps surprisingly, this drastic filtering produces dispersive surface waves with a waveform similar to that of surface waves excited by earthquakes (Shapiro & Campillo 2004). Bensen et al. (2007) give a comprehensive overview and comparison of methods to suppress bursts of energy.

In addition to extracting surface waves from recorded noise, extracting refracted waves is also possible (Mikesell et al. 2009, Mikesell & van Wijk 2011). Interferometric techniques have also been used to increase the signal-to-noise ratio of refracted waves (Mallison et al. 2011, Bharadwaj et al. 2012) and to retrieve waves diffracted at the core-mantle boundary in order to measure deep mantle structure (Ruigrok et al. 2012).

5. INCREASING ILLUMINATION WITH BODY WAVES

Extracting body waves from noise measurements has proven to be much more difficult. Low-frequency P waves (Roux et al. 2005a) and Moho-reflected body waves have been extracted from cross correlation of noise (Zhan et al. 2010, Poli et al. 2012). Noise generated by Hurricane Katrina has led to extraction of P waves (Gerstoft et al. 2006), and several studies have shown that oceanic noise generates P waves (Gerstoft et al. 2008, Zhang et al. 2009). Cross correlation of noise in exploration seismology has led to reflected P waves (Draganov et al. 2007, 2009) and S waves (Nakata et al. 2011). In all of these studies, the extracted body waves were of much lower quality than the surface waves extracted from noise. For this reason, the extraction of body waves from noise has not taken the prominent place in seismology that surface-wave interferometry has taken.

Figure 7 illustrates why it is more difficult to extract body waves from noise than it is to retrieve surface waves. **Figure 7*a*** is relevant for the retrieval of surface waves. Any source on the receiver line launches waves that propagate first to receiver *B* and then to receiver *A*. The cross correlation of these waves gives the surface wave that propagates between these receivers, regardless of the exact location of the noise source on the receiver line. The situation for the retrieval of body waves is different. **Figure 7*b*** shows a diving body wave that propagates from *B* to *A*. Receiver *B* does not radiate a body wave, of course, so this body wave can propagate between the receivers in only one way: A noise source *S*, located at just the right distance, launches body waves that, upon reflection by the free surface, propagate as the diving wave from *B* to *A*. The other noise sources do not launch such waves because they are not at the correct location to launch body waves that propagate from *A* to *B*; hence they do not contribute to the extraction of the body wave. The requirements for the presence of noise sources for the retrieval of body waves are thus more stringent than for the retrieval of surface waves. Halliday & Curtis (2008) show that for the retrieval of higher-mode surface waves, one needs a more extensive distribution of noise sources than is needed for

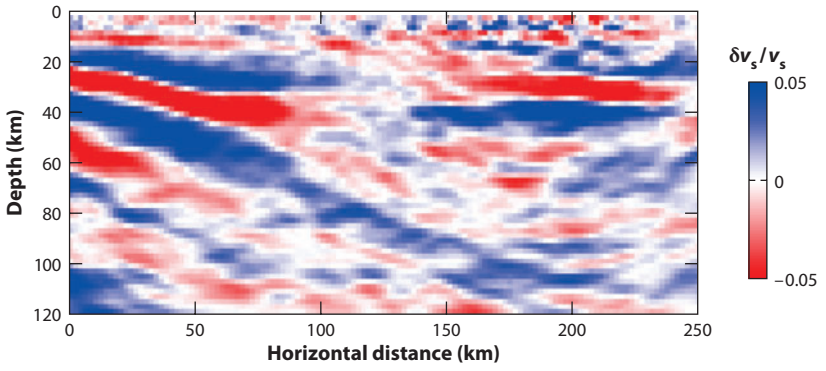

Figure 8

Image of the Cascadia subduction zone created from reflected waves that were retrieved from teleseismic body waves (Bostock et al. 2002).

the fundamental mode. Theory has shown that the convergence of the correlations toward the Green's function (or impulse response) is slower in 3D (bulk waves) than in 2D (Larose et al. 2008). Because noise is not generated everywhere along Earth's surface, extracting body waves has proven more difficult than retrieving surface waves (Forghani & Snieder 2010).

There are two ways out of this conundrum. The first way to retrieve body waves that propagate between sensors is to use downhole sensors (**Figure 5*b***). Using downhole sensors with either controlled surface sources (Bakulin & Calvert 2006, Bakulin et al. 2007) or random noise (Miyazawa et al. 2008) has led to what is known as the virtual source method in exploration seismology. This method removes the imprint of a complicated overburden and allows for illumination of the subsurface that could not be obtained otherwise. The virtual source method has been used, for example, to illuminate the flanks of salt domes from sensors in a vertical borehole (Xiao et al. 2006, Hornby & Yu 2007) and to eliminate waves reflected at Earth's surface (Mehta et al. 2007a). Gerry Schuster, in particular, has pioneered interferometric methods to increase illumination of the subsurface (Schuster et al. 2004; Schuster 2005, 2009).

The second way to retrieve body waves is to use sources that launch waves upward toward sensors at the surface (**Figure 5*a***). The body waves reflected by the free surface can then be used to probe Earth's interior. This principle has been applied using teleseismic body waves as a source for waves reflected in the crust (Bostock & Sacchi 1997, Bostock 1999, Bostock et al. 2002, Kumar & Bostock 2006). Although the method of Bostock and coworkers is based on the concept of Claerbout (1968) to convert transmission data into reflection data, they used multichannel deconvolution rather than cross correlation in their implementation. **Figure 8** shows an image of the Cascadia subduction zone obtained from this principle. The subducting slab and the base of the crust are clearly visible.

Body waves have also been successfully extracted through the use of earthquakes that illuminate a borehole sensor and the surface sensor from below; an early example of this principle from Trampert et al. (1993) is shown in **Figure 6**. This principle has been applied to the detection of time-lapse changes in the near surface by Sawazaki et al. (2009). Nakata & Snieder (2011) applied deconvolution of earthquake signals recorded in borehole sensors and surface sensors at KiK-net stations, giving S waves that propagate between sensors. **Figure 9** shows the highly stable S waves extracted from different earthquakes at a station in Fukushima, Japan. During the Tohoku-oki earthquake on March 11, 2011, the S wave was strongly delayed; this delay indicates that the shaking softened the soil. In the two months after the Tohoku-oki event, the extracted

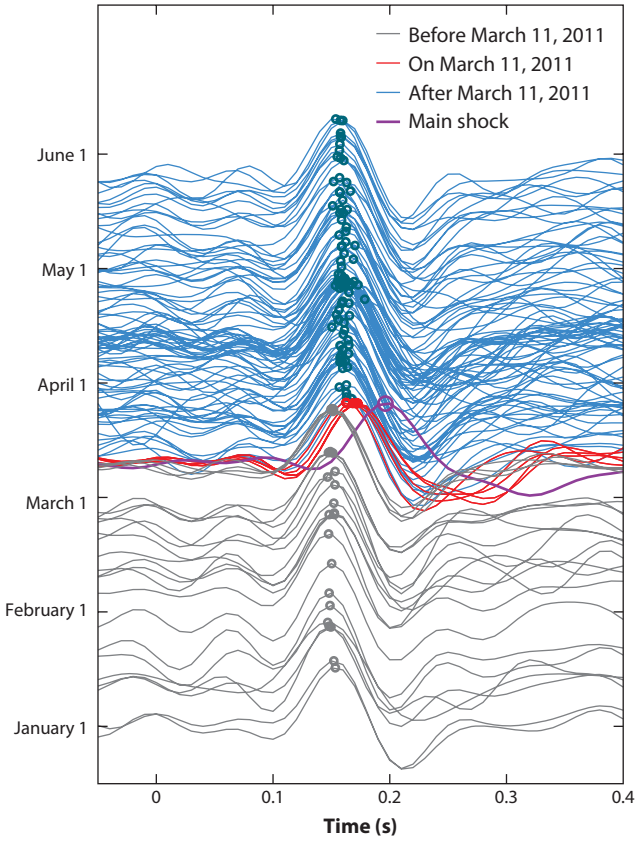

Figure 9

The waveforms recorded for different earthquakes at the surface at KiK-net station FKSH18 (Fukushima). The waveforms deconvolved with the waves recorded in a borehole 100 m deep before the Tohoku-oki event on March 11, 2011 (*gray traces*), on the day of the event (*red traces*), and after the event (*blue traces*). The deconvolved waves for the Tohoku-oki event are shown in purple. Circles indicate the maximum of each trace; the times of these maxima are used to estimate velocity variations.

shear waves still have a residual delay, which corresponds to a reduction of the shear modulus. In the next section, we further investigate the possibility of using repetitive noise-based correlation imaging to track temporal changes of the subsurface.

6. TIME-LAPSE MONITORING OF THE NEAR SURFACE

The continuous presence of noise makes it possible to extract the Earth response on a quasi-continuous basis. In practice, the reason that the Earth response cannot be retrieved continuously is that one needs to time-average the cross correlation over a certain period of time (Larose et al. 2008), from a few hours (Miyazawa et al. 2008) to several months (Shapiro & Campillo 2004). This time-averaging makes it possible to detect time-lapse changes on the scale of at least the averaging period. An interesting point is that the noise sources do not need to be perfectly distributed in order for the medium changes to be monitored (Hadziioannou et al. 2009). In other words, noise-based time-lapse monitoring requires less restrictive conditions than those required by noise-based imaging.

Early examples of time-lapse studies were based on the autocorrelation of recorded noise. The autocorrelation gives the waves that propagate from a sensor into the medium and then propagate back to that sensor. Whether these reflected waves are body waves or surface waves is not clear; hence which part of the subsurface is sampled by these waves is not obvious. Sens-Schönfelder & Wegler (2006) used this technique to detect time-lapse changes at a volcano, Mount Merapi in Indonesia, and discovered that the time-lapse changes they found correlate well with precipitation. This result is an indication that the waves extracted by autocorrelation of noise recorded at the surface propagate through the near surface. Signals extracted from ambient noise or complicated earthquake recordings have been used in several studies to show that the subsurface velocity was reduced after earthquakes in Japan (Wegler & Sens-Schönfelder 2007, Ohmi et al. 2008, Yamada et al. 2010, Nakata & Snieder 2012), as well as after earthquakes at Parkfield (Brenguier et al. 2008a) and Sumatra (Xu & Song 2009). Cross correlation of noise has also been used to monitor changes in Mount St. Helens (Sabra et al. 2006). The prospect of detecting precursors to natural disasters is of particular interest (Brenguier et al. 2008b), and the Earth response extracted with interferometric techniques from noise or earthquakes has shown that the shear-wave velocity in the near surface displays a seasonal cycle (Meier et al. 2010, Nakata & Snieder 2012).

6.1. Monitoring of a Landslide

Characterizing landslides, along with predicting their failure, is of critical importance for society. In most cases, failure is associated with hydrogeological features. Unfortunately, the converse does not hold: An increase in moisture and/or water-table level does not necessarily trigger slope failure. Because seismic waves are sensitive to the mechanical properties of the material they traverse, they are useful for monitoring the evolution of the rigidity (and rheology) of the slope. Ambient noise correlation is promising, as it is quasi-continuous and does not rely on a reproducible controlled source.

Mainsant et al. (2012) studied a clay-rich landslide located in the Swiss Alps, next to the ski resort Les Diablerets and along the road leading to the highly frequented Le Pillon pass. The purpose of the seismic noise correlation experiment was to monitor the failure of this slope, which occurred between August 18 and August 20, 2010, following significant cumulative rainfall in July. The geometry of the experiment is depicted in **Figure 10**. The landslide is of moderate size; it is 100 m in height, has a length of 300 m, and has 20–40 m of lateral extension. It was equipped with two seismic sensors located on each side, on stable ground. Both sensors were connected to the same recording system for continuous data logging. Researchers studied records in the 4–25-Hz frequency range, which corresponds to Rayleigh wave penetration depths ranging from a few meters to a few tens of meters, thus probing the active shallow layers of the landslide. From direct observations during the field experiments, two main sources of ambient noise were identified in this frequency band: the wind in the trees and the traffic along the road at the foot of the landslide. Although the noise from both sources may be variable in time, the important feature for monitoring is that their locations are stable (Hadziioannou et al. 2009).

The 24-h cross correlations were calculated and averaged each day. Correlations were subsequently filtered in a narrow 10–14-Hz frequency band before the relative velocity change was analyzed. In the case of a homogeneous relative velocity change $\delta v/v$, all the waveforms constituting the correlograms are extended in time by a factor of $-\delta v/v$. The relative velocity change between subsequent days was measured with the stretching technique (Sens-Schönfelder & Wegler 2006, Hadziioannou et al. 2009).

Variation of velocity versus time is displayed in **Figure 11**, along with the daily precipitation. From the beginning of April to the middle of July 2010, the apparent Rayleigh wave velocity was

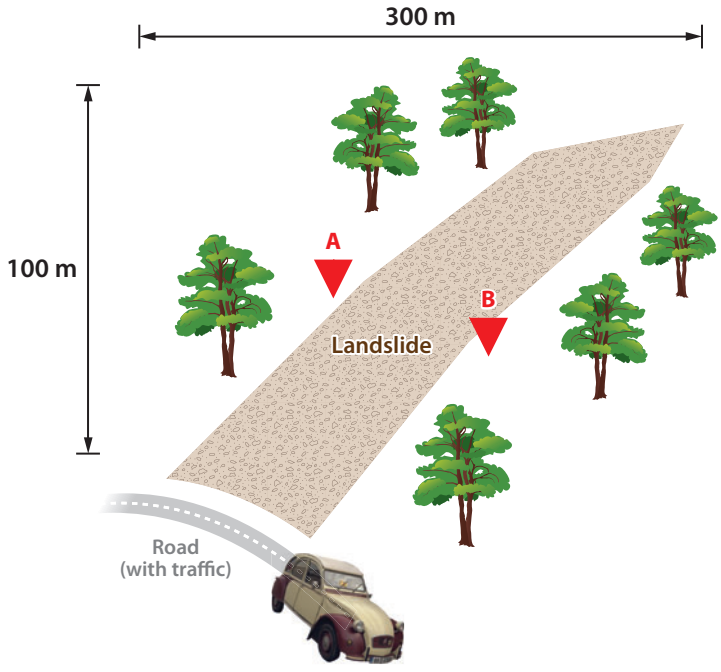

Figure 10

Locations of seismometers (*red triangles*) and landslide area (*brown*) associated with a clay-rich landslide in the Swiss Alps, near the ski resort Les Diablerets.

relatively stable: Observed velocity fluctuations are smaller than 1%. From mid-May to mid-July, rainfall increased the water content of the soil. On July 24, after a short rainfall event, the apparent Rayleigh wave velocity underwent a gradual decrease of 2% over 20 days. On August 15, after a series of intense precipitation events and related increases in the water table, the apparent velocity dropped by 7% in only four days. While losing its rigidity, the creeping material reached its stability limit and the slope failed, with a composite earth slide–earthflow event. This catastrophic event occurred between August 18 and 20 (**Figure 11**). Ambient noise measurements and processing made it possible to observe a significant drop (7%) in Rayleigh wave velocity a few days before the event, after an initial gentler decrease (2%). The observed significant drop in seismic velocity prior to slope failure suggests that time-dependent variation in this parameter can be a valuable precursor to landslide failure.

6.2. Extracting the Lunar Response

The ambient noise on Earth is controlled primarily by the oceanic activity below 1 Hz and by the weather and the human activity above 1 Hz. Imagine now a seismic experiment in which all those sources would be deactivated. What would the noise correlations resemble? Would they still provide information on the subsoil? Of course, such an experiment is not possible on Earth, but it can be carried out on the Moon. During the Apollo era, seismic devices were operated continuously during a significant amount of time to test the noise-based imaging and monitoring techniques. The set of data collected by the Apollo 17 mission is of particular interest.

The Apollo 17 Lunar Seismic Profiling Experiment (LSPE) was deployed on December 14, 1972, at a distance of approximately 180 m west-northwest of the lunar module. Four geophones,

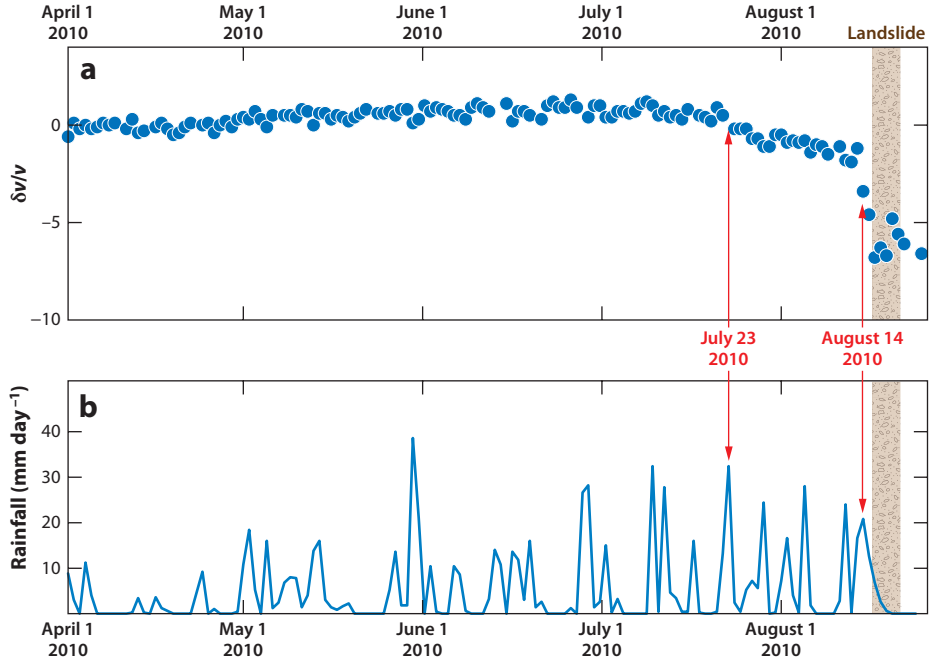

Figure 11

(*a*) Relative velocity change and (*b*) precipitation as a function of time for the Swiss Alps landslide. The landslide occurred in the time interval marked with the brown bar. Vertical red arrows indicate times of strong rainfall.

deployed in a triangular array (**Figure 12*a***), recorded the vertical ground velocity in the 3–30-Hz frequency range during the landing mission in 1972 and then again continuously from August 1976 to April 1977. The geophones were simultaneously connected to the central station, where the seismic signals were digitized and telemetered to Earth. The cross correlations between all pairs of geophones were computed in a procedure that gave the propagation of the direct Rayleigh wave in the lunar regolith (**Figure 12*b***). The dispersion properties of the Rayleigh wave made it possible to determine the shear-wave velocity profile of the first 10 m of the superficial lunar regolith (**Figure 12*c***). More details on the experiment and data processing are given by Larose et al. (2005).

As the seismic noise was almost continuously excited, processing correlations on a 24-h basis was also possible. The comparison between each daily correlation and the correlation averaged over the whole period of interest allowed us to measure the relative velocity variations (Sens-Schönfelder & Larose 2008). These variations are related to the thermal heating of the Sun. During the lunar day, the surface temperature increases by more than 250°C. The heat then slowly diffuses at depth, and the elastic moduli subsequently decrease, resulting in a decrease in apparent Rayleigh wave velocity (**Figure 13**). Conversely, during the lunar night, the temperature decreases and the seismic velocity increases. Variations of energy inflow due to changes in the Sun-Moon distance are reflected by the variations in the incident solar flux (**Figure 13**). This experiment demonstrates that it is possible to evaluate the change of temperature in the lunar soil from the correlation of ambient seismic noise. These experiments demonstrate not only that we can reconstruct direct waves between passive sensors with ambient noise, but also that we can take

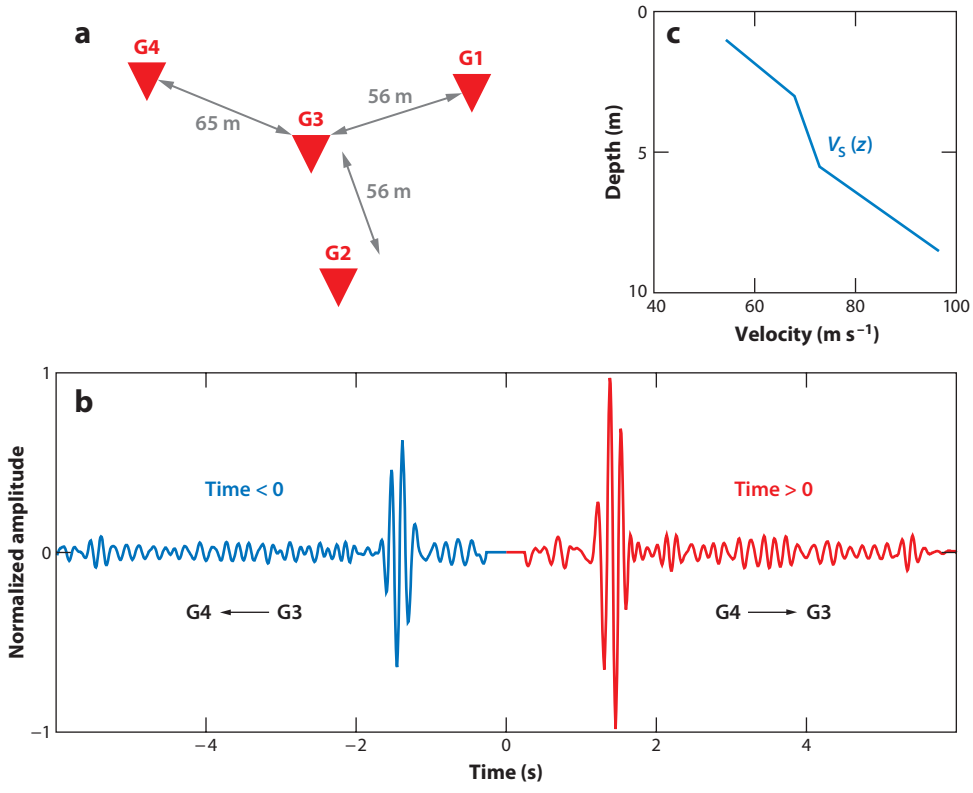

Figure 12

(*a*) Configuration of the four geophones (G1–G4) spread in a triangular array at the Apollo 17 landing site. (*b*) Example of positive ambient noise correlations between G3 and G4. The pulse around 1.5 s is the direct Rayleigh wave between the geophones. (*c*) The shear-wave velocity [$V_s(z)$] profile of the subsoil under the sensors inferred from the dispersion of Rayleigh waves.

advantage of reconstructed multiply scattered waves to monitor very weak changes in a complex natural environment.

7. CONCLUSION

The field of seismic interferometry (also known as Green's function extraction or Green's function retrieval, as discussed) is still rapidly progressing, and this review cannot do justice to all the developments taking place. Multiple schemes for extracting the Earth response are being exploited. In this review, we have mentioned the use of correlation, deconvolution (Vasconcelos & Snieder 2008a,b), and cross coherence. In addition to these methods, two other approaches have been proposed. In multidimensional deconvolution (Wapenaar et al. 2008b, 2011b; van der Neut et al. 2011) one decomposes a recorded elastic or electromagnetic wave field into upgoing and downgoing fields and solves for the reflectivity by solving a linear system of equations. Slob & Wapenaar (2007) proposed convolution interferometry, a technique that is appropriate when the receivers are on opposite sides of a surface that contains the noise sources. The merits and drawbacks of different approaches are discussed by Snieder et al. (2009). Nakata et al. (2011) compare the statistical properties of cross correlation, deconvolution, and cross coherence. In general, a

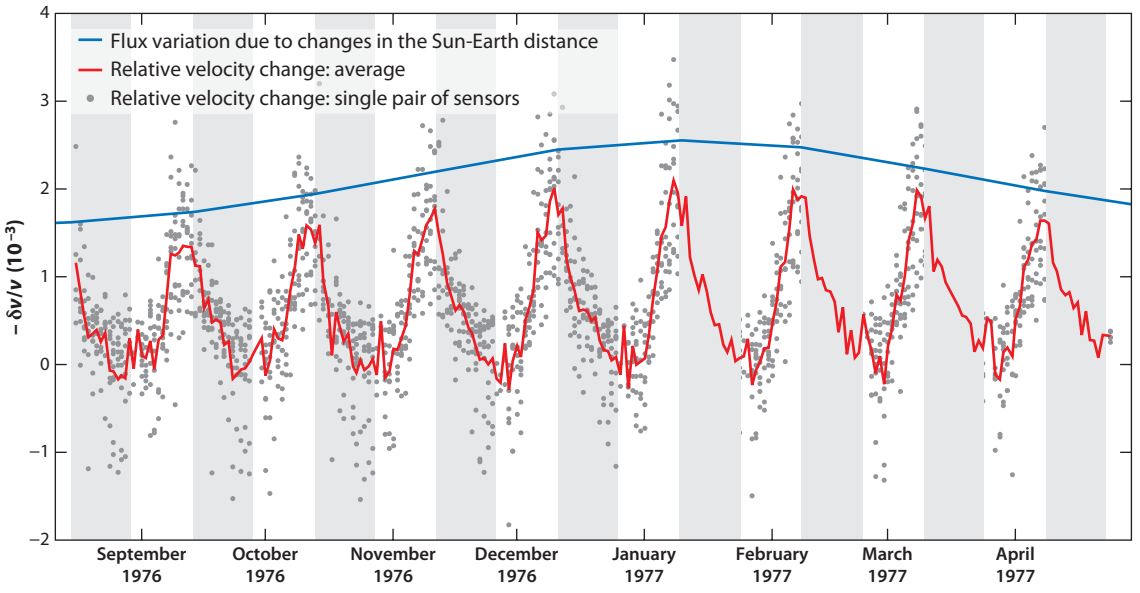

Figure 13

Relative velocity variations ($\delta v/v$) versus time, obtained on the Moon from August 1976 to May 1977. Gray points indicate experimental measurements. The red line indicates the average of $\delta v/v$ over all available pairs of sensors. The blue line is linearly proportional to the Sun-Earth distance. Note the negative sign of the $\delta v/v$ on the vertical axis.

straightforward cross correlation or deconvolution does not optimally focus energy onto the receiver that acts as a virtual source. When noise is recorded on an array, the formalism of multidimensional deconvolution can be used to optimize the focusing of the noise on the receiver that acts as a virtual source (van der Neut & Bakulin 2009; Wapenaar & van der Neut 2010; Wapenaar et al. 2011a,b).

Seismic interferometry has been used for numerous unexpected applications. Recorded ambient oceanic noise has been used for the localization of stations and calibration of their clocks (Sabra et al. 2005c), and to correct for the time drift of seismic stations (Stehly et al. 2007). We have shown examples of receivers that can act as virtual sources, but one can also turn seismic sources into virtual receivers (Curtis et al. 2009). Retrieving the waves propagating between sources from measurements of the energy flux is also possible (Snieder et al. 2012). Furthermore, seismic noise has been used to locate earthquakes (Barmin et al. 2011). Correlation of coda waves that are themselves obtained from cross correlation can be used to compensate for deficiencies in illumination by ambient noise (Stehly et al. 2008, Froment et al. 2011). A method relying on fiducial stations has been developed to estimate the waves that propagate between seismic sensors that were not deployed at the same time (Ma & Beroza 2012), and as shown by Curtis et al. (2012), seismic interferometry can even be used to reconstruct data that were never recorded!

DISCLOSURE STATEMENT

The authors are not aware of any affiliations, memberships, funding, or financial holdings that might be perceived as affecting the objectivity of this review.

APPENDIX A: DERIVATION OF EQUATIONS (7) AND (8)

Using the integral representation theorem of the Bessel function [expression 11.30c of Arfken & Weber (2001)] yields the equation $2\pi J_0(\xi) = \int_0^{2\pi} \exp(i\xi \cos\varphi) d\varphi$, with J_0 the Bessel function of order zero. The Bessel function can be decomposed into the Hankel function of the first and second kind using $J_0(kR) = (1/2)[H_0^{(1)}(kR) + H_0^{(2)}(kR)] = (1/2)[H_0^{(1)}(kR) + H_0^{(1)*}(kR)]$, where expressions 11.85 and 11.86 of Arfken & Weber (2001) have been used. These results reduce Equation (6) to

$$\langle u_A u_B^* \rangle = \pi |S|^2 [H_0^{(1)}(kR) + H_0^{(1)*}(kR)]. \tag{15}$$

The Green's function for wave propagation in a 2D homogeneous medium is given by $G_{2D}(R) = (-i/4)H_0^{(1)}(kR)$ [expression 19.43 of Snieder (2004a)]. Inserting this in Equation (15) gives Equation (7).

The derivation is actually simpler in 3D; the geometry of this problem is shown in **Figure 1*c***. Following steps resembling those leading to Equation (6) gives, for this case,

$$\langle u_A u_B^* \rangle = |S|^2 \varphi \int_0^{\pi} \int_0^{2\pi} e^{ikR\cos\theta} d\varphi \sin\theta d\theta, \tag{16}$$

where θ is the angle between the direction of plane-wave propagation and the line between the receivers (now the z-axis). Instead of the integration over the unit circle in Equation (6), we now integrate over the unit sphere that describes the directions of the incoming waves. The integration over φ gives a multiplication with 2π, and the integration over θ is given by $\int_0^{\pi} e^{ikR\cos\theta} \sin\theta d\theta = \int_{-1}^{1} e^{ikRu} du = (e^{ikR} - e^{-ikR})/(ikR)$. Inserting these results into Equation (16) gives Equation (8).

APPENDIX B: DERIVATION OF EQUATION (10), THE FLUCTUATION RESPONSE THEOREM

The expectation value of a parameter $f(A_i)$ is given by (Le Bellac et al. 2004)

$$\langle f(A_i) \rangle = \frac{Tr\left(f(A_i) \exp\left(\sum_k \lambda_k A_k\right)\right)}{Tr\left(\exp\left(\sum_k \lambda_k A_k\right)\right)}, \tag{17}$$

where Tr denotes the trace, defined as a sum over all degrees of freedom. With this definition, the expectation value of A_i is given by

$$\langle A_i \rangle = \frac{Tr\left(A_i \exp\left(\sum_k \lambda_k A_k\right)\right)}{Tr\left(\exp\left(\sum_k \lambda_k A_k\right)\right)} = \frac{Tr\left(\frac{\partial}{\partial \lambda_i} \exp\left(\sum_k \lambda_k A_k\right)\right)}{Tr\left(\exp\left(\sum_k \lambda_k A_k\right)\right)} = \frac{1}{Z}\frac{\partial Z}{\partial \lambda_i}, \tag{18}$$

where the partition function Z is defined by

$$Z = Tr\left(\exp\left(\sum_k \lambda_k A_k\right)\right). \tag{19}$$

Differentiating Equation (18) with respect to λ_j gives

$$\frac{\partial \langle A_i \rangle}{\partial \lambda_j} = \frac{1}{Z}\frac{\partial^2 Z}{\partial \lambda_i \partial \lambda_j} - \frac{1}{Z^2}\frac{\partial Z}{\partial \lambda_i}\frac{\partial Z}{\partial \lambda_j}. \tag{20}$$

It follows from Equation (18) that the last term is equal to $\langle A_i \rangle \langle A_j \rangle$. The first term on the right-hand side follows from the identities

$$\frac{\partial^2 Z}{\partial \lambda_i \partial \lambda_j} = \frac{\partial^2}{\partial \lambda_i \partial \lambda_j} Tr\left(\exp \sum_k \lambda_k A_k\right) = Tr\left(A_i A_j \exp \sum_k \lambda_k A_k\right) = \langle A_i A_j \rangle Z, \tag{21}$$

where Equations (17) and (19) are used in the last identity. Using these results reduces Equation (20) to

$$\frac{\partial \langle A_i \rangle}{\partial \lambda_j} = \langle A_i A_j \rangle - \langle A_i \rangle \langle A_j \rangle. \tag{22}$$

With the identity $\langle A_i A_j \rangle - \langle A_i \rangle \langle A_j \rangle = \langle (A_i - \langle A_i \rangle)(A_j - \langle A_j \rangle) \rangle$, this gives Equation (10).

LITERATURE CITED

Aki K. 1957. Space and time spectra of stationary stochastic waves with special reference to microtremors. *Bull. Earthq. Res. Inst.* 35:415–56

Arfken GB, Weber HJ. 2001. *Mathematical Methods for Physicists*. Amsterdam: Harcourt. 5th ed.

Bakulin A, Calvert R. 2006. The virtual source method: theory and case study. *Geophysics* 71:SI139–50

Bakulin A, Mateeva A, Mehta K, Jorgensen P, Ferrandis J, et al. 2007. Virtual source applications to imaging and reservoir monitoring. *Lead. Edge* 26:732–40

Barmin MP, Levshin AL, Yang Y, Ritzwoller MH. 2011. Epicentral location based on Rayleigh wave empirical Green's Functions from ambient seismic noise. *Geophys. J. Int.* 184:869–84

Bensen GD, Ritzwoller MH, Barmin MP, Levshin AL, Lin F, et al. 2007. Processing seismic ambient noise data to obtain reliable broad-band surface wave dispersion measurements. *Geophys. J. Int.* 169:1239–60

Bharadwaj P, Schuster G, Mallison I, Dai W. 2012. Theory of supervirtual refraction interferometry. *Geophys. J. Int.* 188:263–73

Bleistein N. 1984. *Mathematical Methods for Wave Phenomena*. Orlando, FL: Academic

Bleistein N, Handelsman RA. 1975. *Asymptotic Expansions of Integrals*. New York: Dover

Bostock MG. 1999. Seismic imaging of lithospheric discontinuities and continental evolution. In *Composition, Deep Structure and Evolution of Continents*, ed. RD van der Hilst, WF McDonough, pp. 1–16. Amsterdam: Elsevier

Bostock MG, Hyndman RD, Rondenay S, Peacock SM. 2002. An inverted continental Moho and serpentinization of the forearc mantle. *Nature* 417:536–38

Bostock MG, Sacchi MD. 1997. Deconvolution of teleseismic recordings for mantle structure. *Geophys. J. Int.* 129:143–52

Brenguier F, Campillo M, Hadziioannou C, Shapiro N, Larose E. 2008a. Postseismic relaxation along the San Andreas Fault at Parkfield from continuous seismological observations. *Science* 321:1478–81

Brenguier F, Shapiro NM, Campillo M, Ferrazzini V, Duputel Z, et al. 2008b. Towards forecasting volcanic eruptions using seismic noise. *Nat. Geosci.* 1:126–30

Bussat S, Kugler S. 2011. Offshore ambient noise surface-wave tomography above 0.1 Hz and its applications. *Lead. Edge* 30:514–24

Callen HB, Welton TA. 1951. Irreversibility and generalized noise. *Phys. Rev.* 83:34–40

Campillo M, Paul A. 2003. Long-range correlations in the diffuse seismic coda. *Science* 299:547–49

Campillo M, Sato H, Shapiro NM, van der Hilst RD. 2011. New developments on imaging and monitoring with seismic noise. *C. R. Geosci.* 343:487–95

Claerbout JF. 1968. Synthesis of a layered medium from its acoustic transmission response. *Geophysics* 33:264–69

Curtis A, Behr E, Entwhistle Y, Galetti E, Townend J, Bannister S. 2012. The benefit of hindsight in observational science: retrospective seismological observations. *Earth. Planet. Sci. Lett.* 345–48:212–20

Curtis A, Gerstoft P, Sato H, Snieder R, Wapenaar K. 2006. Seismic interferometry—turning noise into signal. *Lead. Edge* 25:1082–92

Curtis A, Nicolson H, Halliday D, Trampert J, Baptie B. 2009. Virtual seismometers in the subsurface of the Earth from seismic interferometry. *Nat. Geosci.* 2:700–4

de Ridder S, Dellinger J. 2011. Ambient noise eikonal tomography for near-surface imaging at Valhall. *Lead. Edge* 30:506–12

Draganov D, Campman X, Thorbecke J, Verdel A, Wapenaar K. 2009. Reflection images from ambient seismic noise. *Geophysics* 74:A63–67

Draganov D, Wapenaar K, Mulder W, Singer J, Verdel A. 2007. Retrieval of reflections from seismic background-noise measurements. *Geophys. Res. Lett.* 34:L04305
Duroux A, Sabra KG, Ayers J, Ruzzene M. 2010. Extracting guided waves from cross-correlations of elastic diffuse fields: applications to remote structural health monitoring. *J. Acoust. Soc. Am.* 127:204–15
Duvall TL, Jefferies SM, Harvey JW, Pomerantz MA. 1993. Time-distance helioseismology. *Nature* 362:430–32
Einstein A. 1906. Zur Theorie der Brownschen Bewegung. *Ann. Phys.* 19:371–81
Ekström G, Abers GA, Webb SC. 2009. Determination of surface-wave phase velocities across USArray from noise and Aki's spectral formulation. *Geophys. Res. Lett.* 36:L18301
Forghani F, Snieder R. 2010. Underestimation of body waves and feasibility of surface-wave reconstruction by seismic interferometry. *Lead. Edge* 29:790–94
Froment B, Campillo M, Roux P. 2011. Reconstructing the Green's function through iteration of correlations. *C. R. Geosci.* 343:623–32
Galetti E, Curtis A. 2012. Generalised receiver functions and seismic interferometry. *Tectonophysics* 532–35:1–26
Gallot T, Catheline S, Roux P, Brum J, Benech N, Negreira C. 2011. Passive elastography: shear wave tomography from physiological noise correlation in soft tissues. *IEEE Trans. Ultrason. Ferroelectr. Freq. Control* 58:1122–26
Gerstoft P, Fehler MC, Sabra KG. 2006. When Katrina hit California. *Geophys. Res. Lett.* 33:L17308
Gerstoft P, Shearer PM, Harmon N, Zhang J. 2008. Global P, PP, and PKP wave microseisms observed from distant storms. *Geophys. Res. Lett.* 35:L23306
Gouédard P, Stehly L, Brenguier F, Campillo M, Colin de Verdière Y, et al. 2008. Cross-correlation of random fields: mathematical approach and applications. *Geophys. Prospect.* 56:375–93
Greene RF, Callen HB. 1951. On the formulation of thermodynamic fluctuation theory. *Phys. Rev.* 83:1231–35
Haas A, Revil A. 2009. Electrical burst signature of pore-scale displacements. *Water Resour. Res.* 45:W10202
Hadziioannou C, Larose E, Coutant O, Roux P, Campillo M. 2009. Stability of monitoring weak changes in multiply scattering media with ambient noise correlation: laboratory experiments. *J. Acoust. Soc. Am.* 125:3688–95
Halliday D, Curtis A. 2008. Seismic interferometry, surface waves and source distribution. *Geophys. J. Int.* 175:1067–87
Halliday D, Curtis A, Kragh E. 2008. Seismic surface waves in a suburban environment: active and passive interferometric methods. *Lead. Edge* 27:210–18
Halliday DF, Curtis A, Robertsson JOA, van Manen D-J. 2007. Interferometric surface-wave isolation and removal. *Geophysics* 72:A69–73
Haney MM. 2009. Infrasonic ambient noise interferometry from correlations of microbaroms. *Geophys. Res. Lett.* 36:L19808
Hornby BE, Yu J. 2007. Interferometric imaging of a salt flank using walkaway VSP data. *Lead. Edge* 26:760–63
Johnson JB. 1928. Thermal agitation of electricity in conductors. *Phys. Rev.* 32:97–109
Kohler MD, Heaton TH, Bradford SC. 2007. Propagating waves in the steel, moment-frame Factor building recorded during earthquakes. *Bull. Seismol. Soc. Am.* 97:1334–45
Kubo R. 1966. The fluctuation-dissipation theorem. *Rep. Prog. Phys.* 29:255–84
Kumar MR, Bostock MG. 2006. Transmission to reflection transformation of teleseismic wavefields. *J. Geophys. Res.* 111:B08306
Larose E. 2006. Mesoscopics of ultrasound and seismic waves: application to passive imaging. *Ann. Phys. Fr.* 31:1–126
Larose E, Derode A, Campillo M, Fink M. 2004. Imaging from one-bit correlations of wideband diffuse wave fields. *J. Appl. Phys.* 95:8393–99
Larose E, Khan A, Nakamura Y, Campillo M. 2005. Lunar subsurface investigated from correlation of seismic noise. *Geophys. Res. Lett.* 32:L16201
Larose E, Margerin L, Derode A, van Tiggelen B, Campillo M, et al. 2006a. Correlation of random wavefields: an interdisciplinary review. *Geophysics* 71:SI11–21
Larose E, Montaldo G, Derode A, Campillo M. 2006b. Passive imaging of localized reflectors and interfaces in open media. *Appl. Phys. Lett.* 88:104103

Larose E, Roux P, Campillo M, Derode A. 2008. Fluctuations of correlations and Green's function reconstruction: role of scattering. *J. Appl. Phys.* 103:114907
Lawrence JF, Prieto GA. 2011. Attenuation tomography of the western United States from ambient seismic noise. *J. Geophys. Res.* 116:B06302
Le Bellac M, Mortessagne F, Batrouni GG. 2004. *Equilibrium and Non-Equilibrium Statistical Thermodynamics*. Cambridge, UK: Cambridge Univ. Press
Li HY, Su W, Wang ZX, Huang CY. 2009. Ambient noise Rayleigh wave tomography in western Sichuan and eastern Tibet. *Earth Planet. Sci. Lett.* 282:201–11
Lin F, Moschetti MP, Ritzwoller MH. 2008. Surface wave tomography of the western United States from ambient noise: Rayleigh and Love wave phase velocity maps. *Geophys. J. Int.*173:281–98
Lin FC, Ritzwoller MH, Snieder R. 2009. Eikonal tomography: surface wave tomography by phase front tracking across a regional broad-band seismic array. *Geophys. J. Int.* 177:1091–110
Lobkis OI, Weaver RL. 2001. On the emergence of the Green's function in the correlations of a diffuse field. *J. Acoust. Soc. Am.* 110:3011–17
Ma S, Beroza GC. 2012. Ambient-field Green's functions from asynchronous seismic observations. *J. Geophys. Res.* 39:L06301
Mainsant G, Larose E, Brönnimann, Jongmans D, Michoud C, Jaboyedoff M. 2012. Ambient seismic noise monitoring of a clay landslide: toward failure prediction. *J. Geophys. Res.* 117:F01030
Malcolm A, Scales J, van Tiggelen BA. 2004. Extracting the Green's function from diffuse, equipartitioned waves. *Phys. Rev. E* 70:015601
Mallison I, Bharadwaj P, Schuster G, Jakubowicz J. 2011. Enhanced refractor imaging by supervirtual interferometry. *Lead. Edge* 30:546–50
Mehta K, Bakulin A, Sheiman J, Calvert R, Snieder R. 2007a. Improving the virtual source method by wavefield separation. *Geophysics* 72:V79–86
Mehta K, Snieder R, Graizer V. 2007b. Downhole receiver function: a case study. *Bull. Seismol. Soc. Am.* 97:1396–403
Mehta K, Snieder R, Graizer V. 2007c. Extraction of near-surface properties for a lossy layered medium using the propagator matrix. *Geophys. J. Int.* 168:271–80
Meier U, Shapiro NM, Brenguier F. 2010. Detecting seasonal variations in seismic velocities within Los Angeles basin from correlations of ambient seismic noise. *Geophys. J. Int.* 181:985–96
Mikesell D, van Wijk K. 2011. Seismic refraction interferometry with a semblance analysis on the crosscorrelation gather. *Geophysics* 76:SA77–82
Mikesell S, van Wijk K, Calvert A, Haney M. 2009. The virtual refraction: useful spurious energy in seismic interferometry. *Geophysics* 74:A13–17
Miyazawa M, Snieder R, Venkataraman A. 2008. Application of seismic interferometry to extract P- and S-wave propagation and observation of shear-wave splitting from noise data at Cold Lake, Alberta, Canada. *Geophysics* 73:D35–40
Moschetti MP, Ritzwoller MN, Lin F, Yang Y. 2010. Seismic evidence for widespread western-US deep-crustal deformation caused by extension. *Nature* 464:885–89
Nakata N, Snieder R. 2011. Near-surface weakening in Japan after the 2011 Tohoku-Oki earthquake. *Geophys. Res. Lett.* 38:L17302
Nakata N, Snieder R. 2012. Estimating near-surface shear wave velocities in Japan by applying seismic interferometry to KiK-net data. *J. Geophys. Res.* 117:B01308
Nakata N, Snieder R, Tsuji T, Larner K, Matsuoka T. 2011. Shear wave imaging from traffic noise using seismic interferometry by cross-coherence. *Geophysics* 76:SA97–106
Nishida K, Montagner J-P, Kawakatsu H. 2009. Global surface wave tomography using seismic hum. *Science* 326:112
Nyquist H. 1928. Thermal agitation of electric charge in conductors. *Phys. Rev.* 32:110–13
Ohmi S, Hirahara K, Wada H, Ito K. 2008. Temporal variations of crustal structure in the source region of the 2007 Noto Hanto Earthquake, central Japan, with passive image interferometry. *Earth Planets Space* 60:1069–74
Paul A, Campillo M, Margerin L, Larose E, Derode A. 2005. Empirical synthesis of time-asymmetrical Green functions from the correlation of coda waves. *J. Geophys. Res.* 110:B08302

Poli P, Pedersen HA, Campillo M, POLENET/LAPNET Working Group. 2012. Emergence of body waves from cross-correlation of short period seismic noise. *Geophys. J. Int.* 188:549–58

Prieto GA, Lawrence JF, Beroza GC. 2009. Anelastic earth structure from the coherency of the ambient seismic field. *J. Geophys. Res.* 114:B07303

Prieto GA, Lawrence JF, Chung AI, Kohler MD. 2010. Impulse response of civil structures from ambient noise analysis. *Bull. Seismol. Soc. Am.* 100:2322–28

Rickett JE, Claerbout JF. 2000. Calculation of the sun's acoustic impulse response by multidimensional spectral factorization. *Solar Phys.* 192:203–10

Ritzwoller MH, Lin F-C, Shen W. 2011. Ambient noise tomography with a large seismic array. *C. R. Geosci.* 343:558–70

Roux P, Kuperman WA, NPAL Group. 2004. Extracting coherent wave fronts from acoustic ambient noise in the ocean. *J. Acoust. Soc. Am.* 116:1995–2003

Roux P, Kuperman WA, Sabra KG. 2011. Ocean acoustic noise and passive coherent array processing. *C. R. Geosci.* 343:533–47

Roux P, Sabra KG, Gerstoft P, Kuperman WA. 2005a. P-waves from cross correlation of seismic noise. *Geophys. Res. Lett.* 32:L19303

Roux P, Sabra KG, Kuperman WA, Roux A. 2005b. Ambient noise cross correlation in free space: theoretical approach. *J. Acoust. Soc. Am.* 117:79–84

Ruigrok E, Mikesell D, van Wijk K. 2012. Scanning for velocity anomalies in the crust and mantle with diffractions from the core-mantle boundary. *Geophys. Res. Lett.* 39:L11301

Rytov SM, Kravtsov YuA, Tatarskii VI. 1989. *Principles of Statistical Radiophysics*, Vol. 3: *Elements of Random Fields*. Berlin: Springer-Verlag

Sabra KG, Conti S, Roux P, Kuperman WA. 2007. Passive in vivo elastography from skeletal muscle noise. *Appl. Phys. Lett.* 90:194101

Sabra KG, Gerstoft P, Roux P, Kuperman WA, Fehler MC. 2005a. Extracting time-domain Green's function estimates from ambient seismic noise. *Geophys. Res. Lett.* 32:L03310

Sabra KG, Gerstoft P, Roux P, Kuperman WA, Fehler MC. 2005b. Surface wave tomography from microseisms in Southern California. *Geophys. Res. Lett.* 32:L14311

Sabra KG, Roux P, Gerstoft P, Kuperman WA, Fehler MC. 2006. Extracting coherent coda arrivals from cross-correlations of long period seismic waves during the Mount St. Helens 2004 eruption. *J. Geophys. Res.* 33:L06313

Sabra KG, Roux P, Thode AM, D'Spain GL, Hodgkiss WS, Kuperman WA. 2005c. Using ocean ambient noise for array self-localization and self-synchronization. *IEEE J. Ocean. Eng.* 30:338–47

Sabra KG, Srivastava A, di Scalea FL, Bartoli I, Rizzo P, Conti S. 2008. Structural health monitoring by extraction of coherent guided waves from diffuse fields. *J. Acoust. Soc. Am.* 123:EL8–13

Sawazaki K, Sato H, Nakahara H, Nishimura T. 2009. Time-lapse changes of seismic velocity in the shallow ground caused by strong ground motion shock of the 2000 Western-Tottori earthquake, Japan, as revealed from coda deconvolution analysis. *Bull. Seismol. Soc. Am.* 99:352–66

Scherbaum F. 1987. Levinson inversion of earthquake geometry SH-transmission seismograms in the presence of noise. *Geophys. Prospect.* 35:787–802

Schulte-Pelkum V, Earle PS, Vernon FL. 2004. Strong directivity of ocean-generated seismic noise. *Geochem. Geophys. Geosyst.* 5:Q03004

Schuster GT. 2005. Fermat's interferometric principle for target-oriented traveltime tomography. *Geophysics* 70:U47–50

Schuster GT. 2009. *Seismic Interferometry*. Cambridge, UK: Cambridge Univ. Press

Schuster GT, Yu J, Sheng J, Rickett J. 2004. Interferometric/daylight seismic imaging. *Geophys. J. Int.* 157:838–52

Sens-Schönfelder C, Larose. 2008. Temporal changes in the lunar soil from correlation of diffuse vibrations. *Phys. Rev. E* 78:045601

Sens-Schönfelder C, Wegler U. 2006. Passive image interferometry and seasonal variations of seismic velocities at Merapi Volcano, Indonesia. *Geophys. Res. Lett.* 33:L21302

Shapiro NM, Campillo M. 2004. Emergence of broadband Rayleigh waves from correlations of the ambient seismic noise. *Geophys. Res. Lett.* 31:L07614

Shapiro NM, Campillo M, Stehly L, Ritzwoller MH. 2005. High-resolution surface-wave tomography from ambient seismic noise. *Science* 307:1615–18

Slob E, Snieder R, Revil A. 2010. Retrieving electric resistivity data from self-potential measurements by cross-correlation. *Geophys. Res. Lett.* 37:L04308

Slob E, Wapenaar K. 2007. GPR without a source: cross-correlation and cross-convolution methods. *IEEE Trans. Geosci. Remote Sens.* 45:2501–10

Snieder R. 2004a. *A Guided Tour of Mathematical Methods for the Physical Sciences*. Cambridge, UK: Cambridge Univ. Press. 2nd ed.

Snieder R. 2004b. Extracting the Green's function from the correlation of coda waves: a derivation based on stationary phase. *Phys. Rev. E* 69:046610

Snieder R. 2006. Retrieving the Green's function of the diffusion equation from the response to a random forcing. *Phys. Rev. E* 74:046620

Snieder R. 2007. Extracting the Green's function of attenuating heterogeneous acoustic media from uncorrelated waves. *J. Acoust. Soc. Am.* 121:2637–43

Snieder R, Douma H, Vasconcelos I. 2012. Extracting the Green's function from measurements of the energy flux. *J. Acoust. Soc. Am.* 131:EL309–15

Snieder R, Miyazawa M, Slob E, Vasconcelos I, Wapenaar K. 2009. A comparison of strategies for seismic interferometry. *Surv. Geophys.* 30:503–23

Snieder R, Şafak E. 2006. Extracting the building response using seismic interferometry: theory and application to the Millikan Library in Pasadena, California. *Bull. Seismol. Soc. Am.* 96:586–98

Snieder R, Sheiman J, Calvert R. 2006a. Equivalence of the virtual source method and wavefield deconvolution in seismic interferometry. *Phys. Rev. E* 73:066620

Snieder R, Slob E, Wapenaar K. 2010. Lagrangian Green's function extraction, with applications to potential fields, diffusion, and acoustic waves. *New J. Phys.* 12:063013

Snieder R, Wapenaar K, Larner K. 2006b. Spurious multiples in seismic interferometry of primaries. *Geophysics* 71:SI111–24

Snieder R, Wapenaar K, Wegler U. 2007. Unified Green's function retrieval by cross-correlation; connection with energy principles. *Phys. Rev. E* 75:036103

Song X. 2010. Preface to the special issue on ambient noise seismology. *Earthq. Sci.* 23:395–96

Stehly L, Campillo M, Froment B, Weaver RL. 2008. Reconstructing Green's function by correlation of the coda of the correlation (C^3) of ambient seismic noise. *J. Geophys. Res.* 113:B11306

Stehly L, Campillo M, Shapiro NM. 2006. A study of seismic noise from long-range correlation properties. *J. Geophys. Res.* 111:B10306

Stehly L, Campillo M, Shapiro NM. 2007. Traveltime measurements from noise correlation: stability and detection of instrumental time-shifts. *Geophys. J. Int.* 171:223–30

Tatarskii VP. 1987. Example of the description of dissipative processes in terms of reversible dynamic equations and some comments on the fluctuation-dissipation theorem. *Sov. Phys. Usp.* 30:134–52

Trampert J, Cara M, Frogneux M. 1993. *SH* propagator matrix and Q_s estimates from borehole- and surface-recorded earthquake data. *Geophys. J. Int.* 112:290–99

Tsai V. 2011. Understanding the amplitudes of noise correlation measurements. *J. Geophys. Res.* 116:B09311

van der Neut J, Bakulin A. 2009. Estimating and correcting the amplitude radiation pattern of a virtual source. *Geophysics* 74:SI27–36

van der Neut J, Thorbecke J, Mehta K, Slob E, Wapenaar K. 2011. Controlled-source interferometric redatuming by crosscorrelation and multidimensional deconvolution in elastic media. *Geophysics* 76:SA63–76

van Wijk K. 2006. On estimating the impulse response between receivers in a controlled ultrasonic experiment. *Geophysics* 71:SI79–84

Vasconcelos I, Snieder R. 2008a. Interferometry by deconvolution, Part 1—Theory for acoustic waves and numerical examples. *Geophysics* 73:S115–28

Vasconcelos I, Snieder R. 2008b. Interferometry by deconvolution: Part 2—Theory for elastic waves and application to drill-bit seismic imaging. *Geophysics* 73:S129–41

Wapenaar K, Draganov D, Robertsson JOA, eds. 2008a. *Seismic Interferometry: History and Present Status*. Geophys. Repr. Ser. 26. Tulsa, OK: Soc. Explor. Geophys.

Wapenaar K, Draganov D, Snieder R, Campman X, Verdel A. 2010a. Tutorial on seismic interferometry: Part 1—Basic principles and applications. *Geophysics* 75:75A195–209
Wapenaar K, Ruigrok E, van der Neut J, Draganov D. 2011a. Improved surface-wave retrieval from ambient seismic noise by multi-dimensional deconvolution. *Geophys. Res. Lett.* 38:L01313
Wapenaar K, Slob E, Snieder R. 2006. Unified Green's function retrieval by cross-correlation. *Phys. Rev. Lett.* 97:234301
Wapenaar K, Slob E, Snieder R. 2008b. Seismic and electromagnetic controlled-source interferometry in dissipative media. *Geophys. Prospect.* 56:419–34
Wapenaar K, Slob E, Snieder R, Curtis A. 2010b. Tutorial on seismic interferometry: Part 2—Underlying theory and new advances. *Geophysics* 75:75A211–27
Wapenaar K, van der Neut J. 2010. A representation for Green's function retrieval by multidimensional deconvolution. *J. Acoust. Soc. Am.* 128:EL366–71
Wapenaar K, van der Neut J, Ruigrok E, Draganov D, Hunziker J, et al. 2011b. Seismic interferometry by crosscorrelation and by multidimensional deconvolution: a systematic comparison. *Geophys. J. Int.* 185:1335–64
Weaver RL. 2008. Ward identities and the retrieval of Green's functions in the correlations of a diffuse field. *Wave Motion* 45:596–604
Weaver RL, Lobkis OI. 2001. Ultrasonics without a source: thermal fluctuation correlations at MHz frequencies. *Phys. Rev. Lett.* 87:134301
Weaver RL, Lobkis OI. 2003a. Elastic wave thermal fluctuations, ultrasonic waveforms by correlation of thermal phonons. *J. Acoust. Soc. Am.* 113:2611–21
Weaver RL, Lobkis OI. 2003b. On the emergence of the Green's function in the correlations of a diffuse field: pulse-echo using thermal phonons. *Ultrasonics* 40:435–39
Weaver RL, Lobkis OI. 2005. Fluctuations in diffuse field-field correlations and the emergence of the Green's function in open systems. *J. Acoust. Soc. Am.* 117:3432–39
Webb SC. 1998. Broadband seismology and noise under the ocean. *Rev. Geophys.* 36:105–42
Wegler U, Sens-Schönfelder C. 2007. Fault zone monitoring with passive image interferometry. *Geophys. J. Int.* 168:1029–33
Xiao X, Zhou M, Schuster GT. 2006. Salt-flank delineation by interferometric imaging of transmitted P- to S-waves. *Geophysics* 71:SI197–207
Xu ZJ, Song X. 2009. Temporal changes of surface wave velocity associated with major Sumatra earthquakes from ambient noise correlation. *Proc. Natl. Acad. Sci. USA* 106:14207–12
Xue Y, Dong S, Schuster GT. 2009. Interferometric prediction and subtraction of surface waves with a nonlinear local filter. *Geophysics* 74:SI1–8
Yamada M, Mori J, Ohmi S. 2010. Temporal changes of subsurface velocities during strong shaking as seen from seismic interferometry. *J. Geophys. Res.* 115:B03302
Yang Y, Ritzwoller MH. 2008. Teleseismic surface wave tomography in the western US using the transportable array component of USArray. *Geophys. Res. Lett.* 5:L04308
Yao HJ, van der Hilst RD, de Hoop MV. 2006. Surface-wave array tomography in SE Tibet from ambient seismic noise and two-station analysis: I. Phase velocity maps. *Geophys. J. Int.*166:732–44
Zhan Z, Ni S, Helmberger DV, Clayton RW. 2010. Retrieval of Moho-reflected shear wave arrivals from seismic noise. *Geophys. J. Int.*182:408–20
Zhang J, Gerstoft P, Shearer PM. 2009. High-frequency P-wave seismic noise driven by ocean winds. *Geophys. Res. Lett.* 36:L09302

Annual Review
of Earth and
Planetary Sciences
Volume 41, 2013

Contents